Experimental and Theoretical Electron Magnetic Resonance Study on Radiation-Induced Radicals in α-L-Sorbose Single Crystals

Gauthier C. A. M. Vanhaelewyn,[†,#] Bjørn Jansen,[‡] Ewald Pauwels,[§] Einar Sagstuen,[‡] Michel Waroquier,[§] and Freddy J. Callens*[,†]

Department of Solid State Sciences, Ghent University, Krijgslaan 281-S1, B-9000 Gent, Belgium, Department of Physics, University of Oslo, P.O. Box 1048 Blindern, N-0316 Oslo, Norway, and Laboratory of Theoretical Physics, Ghent University, Proeftuinstraat 86, B-9000 Gent, Belgium

Received: December 16, 2003; In Final Form: February 12, 2004

α-L-Sorbose single crystals were X-irradiated at 295 K (room temperature). A combined electron paramagnetic resonance (EPR), electron nuclear double resonance (ENDOR), and ENDOR-induced EPR (EI-EPR) study at 120 K revealed a realm of radiation-induced free radicals in this sugar system. In the present work, a pair of closely related radicals is focused on, being dominant immediately after irradiation, but unstable with respect to long time storage or upon warming the samples. A density functional theory (DFT) study was carried out considering the complete hyperfine coupling tensors (principal axes and anisotropic and isotropic couplings) in comparison with the observed electron−proton interactions. This combined approach yielded very plausible models for both radicals, which are formed by a net hydrogen-abstraction from the C3 position of the six-membered sorbose ring. It appears that the difference between the two species is linked to the molecular disorder in the sorbose crystal structure. In addition, DFT calculations of the *g* tensors were performed for the plausible radical conformations.

Introduction

The study of free radicals induced by ionizing radiation in carbohydrates using electron magnetic resonance (EMR) techniques is interesting from many viewpoints. The radicals can be used as indicators for radiation exposure to sugar-containing foodstuffs.[1] Furthermore, sucrose is considered as a good candidate for electron paramagnetic resonance (EPR) dosimetry by many authors.[2,3] More fundamentally, sugar radicals are important for the understanding of radiation damage processes in DNA.[4−6]

Theoretical work concerning the molecular structures of free radicals in a variety of host matrixes has become increasingly popular, largely due to the considerable success of density functional theory (DFT) methods in predicting hyperfine coupling constants to a very good degree of accuracy.[7] Reports discussing radical formation in DNA components and in some isolated sugars have been published recently.[4,8−11]

The literature reveals several experimental studies aiming at the identification of one or more radicals contributing to the, in general, quite complex EPR spectra obtained from irradiated sugars, at RT (room temperature) as well as at lower temperatures. Giving a comprehensive review of the literature with respect to sugar radicals is beyond the scope of this paper, and hence, reference will only be made to a number of papers closely related to the work presented here. Next to the familiar table sugar, the disaccharide sucrose and also its two monosaccharide building stones, i.e., glucose and fructose, have been the subject of several EPR, electron nuclear double resonance (ENDOR), and ENDOR-induced EPR (EI-EPR) investigations.

For glucose, excellent work has been performed about two decades ago by Madden and Bernhard, yielding several proposals for reaction schemes and radical structures.[12,13] Very recently two of the latter models have been confirmed beyond doubt using DFT calculations in which the agreement between the calculated and experimental hyperfine tensor eigenvectors of two β-proton couplings appeared to be the most convincing argument.[14] A discrepancy of 10−15% for the isotropic hyperfine values remained however, although a very good qualitative agreement was obtained.

For sucrose, which is an even more complicated system, extensive EMR studies have been performed by two groups, at RT[15] and around 60 K.[9] Convincing models for the contributing radicals could not be proposed however. Similarly, fructose radicals have attracted recent experimental and theoretical interest.[10,11]

From all of these studies, it became clear that usually a multitude of different radicals are formed in these materials. This should alert people involved in EPR applications with sugars, bearing in mind what happened with the popular alanine-dosimetric system. It was not until detailed EPR/ENDOR and EI-EPR experiments were performed that the 3-fold composite spectrum was discovered[16] and that the full consequences of the composite character of the alanine spectrum are becoming clear, e.g., with respect to sensitivity to light and heat treatments (important for storage).[17,18]

In the present paper, attention is focused on the study of an important intermediate radical dominating the EPR spectra in sorbose immediately after irradiation at room temperature. The interpretation of the experimental data is supported by DFT calculations performed on several plausible radical models.

* To whom correspondence should be addressed. Tel: +32/9/2644352. Fax: +32/9/2644996. E-mail: freddy.callens@ugent.be.
† Ghent University.
‡ University of Oslo.
§ Ghent University.
# Postdoctoral Fellow of the Fund for Scientific Research − Flanders (Belgium) (F. W. O.-Vlaanderen).

10.1021/jp037886o CCC: $27.50
Published on Web 03/18/2004

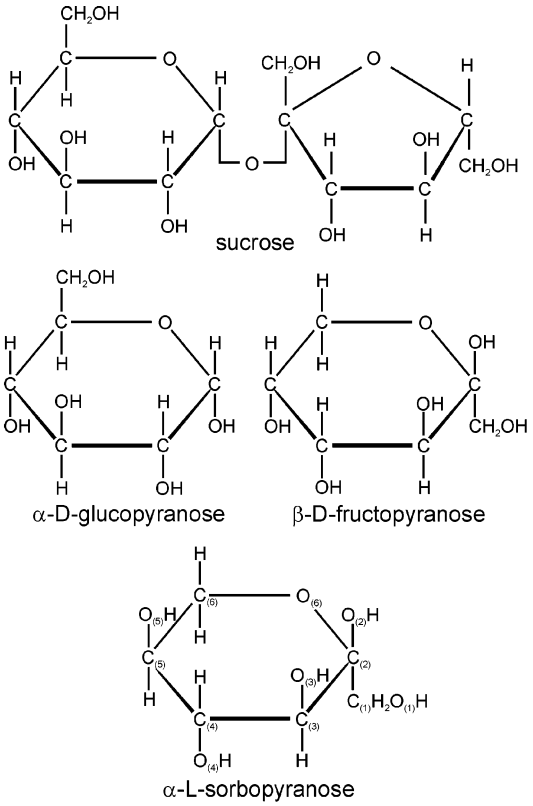

Figure 1. Structures of sucrose, α-D-glucopyranose (glucose), *β*-D-fructopyranose (fructose), and α-L-sorbopyranose (sorbose).

Materials and Methods

Materials. The α-L-sorbose powders were purchased from Aldrich. The crystals used were characterized by X-ray methods and found to check with published crystal structures. The crystals are orthorhombic with space group $P2_12_12_1$ and have 4 molecules per unit cell.[19,20] The *a*, *b*, and *c* axes were chosen as a reference system for both the EMR experiments and the DFT calculations. The sorbose molecules are in the pyranose form which is also the crystalline form for α-D-glucose and *β*-D-fructose. In Figure 1, the most relevant structures for the present study are shown.

For α-L-sorbopyranose (henceforth designated sorbose), crystalline disorder has been found in the orientation of the primary alcohol group between two of the three possible "staggered" positions. As a consequence of this, two sorbose molecular conformations A and B exist in the lattice, each exhibiting one of the two orientations for the primary alcohol (O1−H(O1)). This is apparent in Figure 2, where also the Newman projections along the C1−C2 bonds are given for both conformations. The occupancy of the A and B conformations have been determined by neutron diffraction to be 0.625 and 0.375, respectively.[20]

Experimental Methods. Single crystals of α-L-sorbose were grown from saturated aqueous solutions at room temperature. The crystals were irradiated at RT with X-rays from a Machlett OEG-60 tube operated at 50 kV and 20 mA. The total dose given to the crystals was about 8 kGy. The crystals were then mounted onto a goniometer head of a Weissenberg X-ray diffraction camera. Using oscillation diagrams, the crystal axis parallel to the rotation axis was aligned to within 1°. The crystals were then transferred to a quartz crystal holder for the EPR and ENDOR measurements without loss of alignment.

The X-band EPR and ENDOR experiments were performed at 120 K using a Bruker ER-200 MRD spectrometer having a maximum microwave power of 200 mW. The EPR spectra were recorded with a rectangular cavity working in the TE_{102} mode using 100 kHz modulation frequency, 0.25 mT modulation width, and 30 dB microwave attenuation. The ENDOR accessory was the Bruker EN 200S unit equipped with a 20 W broadband amplifier. The ENDOR experiments were recorded using Bruker's cylindrical ENDOR cavity working in the TM_{011} mode at 12.5 kHz modulation frequency, 100−150 kHz modulation depth and 12−14 dB microwave attenuation. The spectrometer was also equipped with an HP 5342A microwave frequency counter and a Bruker 031M NMR gaussmeter. Data analysis was performed as described previously.[21]

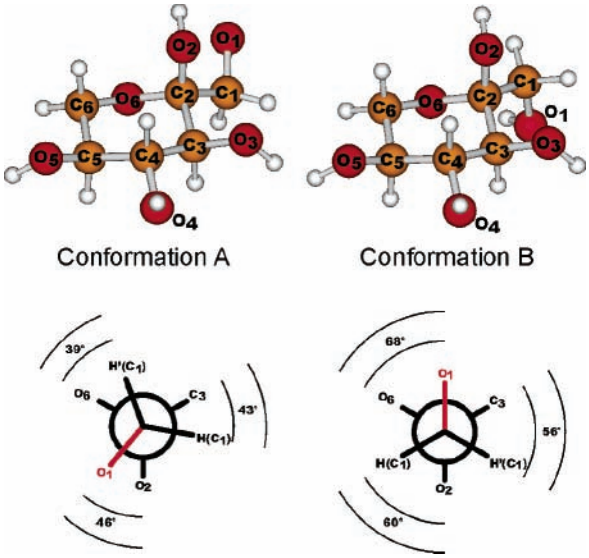

Figure 2. A and B conformations of the sorbopyranose molecules ("No Optimization"), illustrating the disorder in the structure (top) and Newman projections along the C1−C2 bond (bottom).

Computational Details

The general strategy, which was also followed very successfully in the aforementioned paper,[14] should first be outlined. It has to be emphasized that the single molecule approach was used to perform the DFT calculations. This implies that the crystalline molecular environment surrounding the radical was not explicitly incorporated during EPR calculations or geometry optimizations. Calculations on the radical were, therefore, performed in the (ideal) gas phase, at 0 K. The usefulness and feasibility of this method in the calculation of EPR spectroscopic properties has been extensively demonstrated for biomolecules.[8,22−26] The literature reveals several, albeit rather complex and time-consuming, advanced methods to explicitly include the environment for organic radicals.[27,28] In this work, however, we have adopted the single molecule approach in three computational regimes, in which the effect of the crystalline environment has to some extent been taken into account.

The starting points for each of the three methodologies were the initial molecular geometries for the radical models, which were obtained by removing specific atoms from the sorbose crystal structures as determined from neutron diffraction (see below).[20]

In the first step, which is designated as the "No Optimization" regime, all remaining atoms were kept at their original positions in the crystal structure. Keeping the atoms in their original positions in fact reflects the influence of the neighbors in the sense that their positions are determined by all of them.

In the second step, the atoms in the immediate vicinity of the unpaired electron were allowed to relax. More specifically,

only the atoms of the substituent groups being connected with the carbon-centered radical are allowed to relax in the partial geometry optimization action. This computational procedure is in the following designated as the "Partial Optimization" scheme.

Only in the final step, the effect of relaxing all atoms was examined within the "Full Optimization" scheme. One should realize that in a real lattice the radical is not completely free to relax. Since intermolecular hydrogen bonds with lattice sorbose molecules are not taken into account in the single molecule approach, unrealistic reorientations of side chains can occur in the radical. As will be demonstrated in the following, it appears that sometimes optimization within the "Partial Optimization" scheme may provide a result in closer agreement with the experimental data than within the "Full Optimization" scheme. We stress that this statement is not to be generalized, as the results of both latter schemes were shown to be virtually identical in the case of the radiation-induced radicals in glucose.[14]

Within these three computational optimization schemes, all geometry optimizations and EPR calculations were performed on initial radical models created from the A and B sorbose molecular conformations and the results will consequently be discussed in terms of both resulting radical conformations. Calculations were performed using the Gaussian 98 and Gaussian 03 software packages[29,30] within a DFT[31] framework. Molecular orbitals were expanded in a triple-ζ 6-311G(p,d) basis, that is, augmented with single d and p polarization functions,[32,33] and the B3LYP functional[34] was used.

To allow for the determination of the hyperfine tensor principal directions, both geometry optimizations and EPR calculations were performed using the "NoSymm" flag in Gaussian 98. In essence, this was used in order to perform all calculations in the crystal axis reference frame by preventing the Gaussian code to execute an internal reference system transformation. In this way, the calculated tensor directions were generated with respect to the crystal reference frame, which allowed for a direct comparison with the experiment. The latter procedure follows from our aim to establish as good as possible agreement between the experimental and calculated hyperfine coupling tensor principal axes. In the literature, very few examples are known where calculated principal axes are reported and compared with those obtained from ENDOR experiments. One usually aims for a good agreement for the isotropic and anisotropic couplings.[7] The approach adopted here is thus closer to the analysis method of the experimentalist. Evidently, the calculated anisotropic and isotropic hyperfine couplings have to be considered as well, but in a less prominent role than is usually done. Obviously, there are limitations to this rather simple but quite fast and often very efficient approach (discussed in more detail in ref 14), but the authors would like to emphasize that a complete neglect of the analysis on the principal axes might sometimes lead to wrong radical model structures.[35]

Results

Experimental Results. Whereas before irradiation no EPR signals are present, exposure to a few kGy of X-rays leads to strong and quite complex EPR spectra, mainly due to multiple signal overlap. In Figure 3, typical X-band spectra obtained immediately after X irradiation with the magnetic field along the main crystallographic orientations are shown. Although the ENDOR and EI-EPR studies convincingly show that about 10 radical species are contributing to these spectra, the present work is confined to the most prominent doublet which can, e.g., be easily distinguished in Figure 3, parts a and b. This resonance, with a typical splitting of about 2.5 mT, will be labeled R1. In a subsequent paper, a discussion of the other radicals present together with computer simulations of the EPR spectra will be presented.[36]

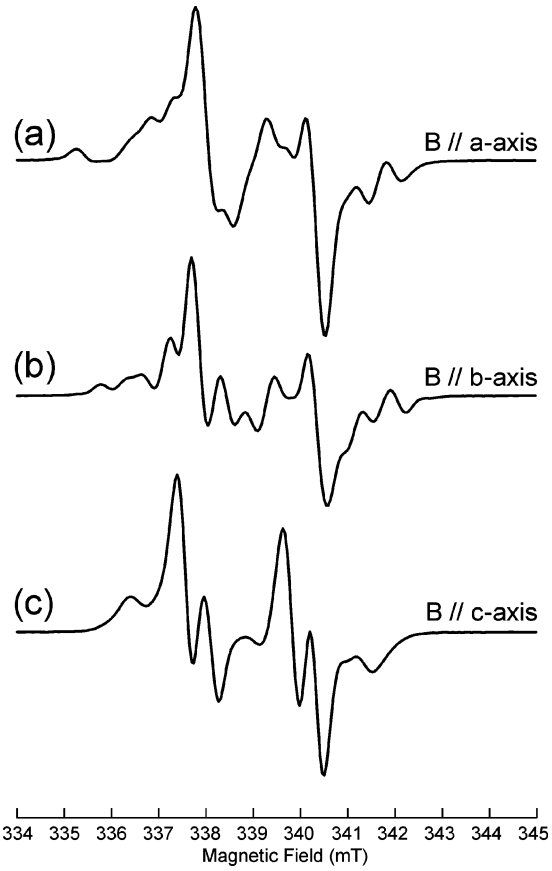

Figure 3. EPR spectrum of X-irradiated α-L-sorbose for the magnetic field parallel to the *a*, *b*, and *c* axes.

By means of EI-EPR, ENDOR lines belonging to the same radical can be isolated and the corresponding EPR spectrum can, in principle, be reconstructed because for a nucleus with $I = {}^1/_2$, the EI-EPR spectrum is similar to the EPR absorption spectrum. The ENDOR lines of R1 were recorded in the *ab*, *bc*, and *ca* planes by rotations along the *c*, *a*, and *b* axes, respectively. Due to the orthorhombic symmetry, site splitting occurs in all three planes of rotation. The thus obtained angular variations of the ENDOR resonance frequencies are shown in Figure 4. This figure also shows the EI-EPR spectra obtained with the magnetic field directed along the main crystallographic axes with the rf frequency locked to the ENDOR transitions corresponding to the two detectable hyperfine interactions of R1. The experimental data have been fit (fully drawn lines in Figure 4) using the deduced ENDOR parameters presented in Table 1a.

Complete angular variations of two very similar β couplings were obtained in the three planes. Furthermore, a third (also similar) coupling was observed in the *bc* plane but could not be observed in the other planes (see discussion below). At first, it was not clear whether those couplings belonged to one radical or whether quite similar radicals, each with only one strong β-coupling, were present. However, the doublet nature of the EPR and EI-EPR spectra with a splitting corresponding to the actual ENDOR frequencies unambiguously showed that in fact similar radicals are observed. As will be further argued below, also the DFT calculations support this conclusion.

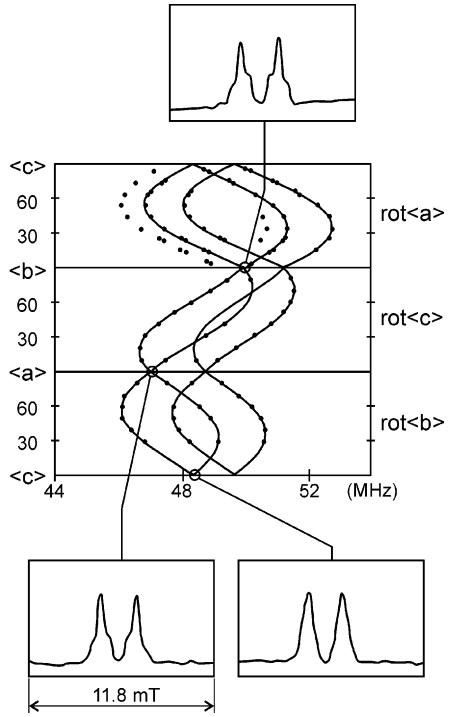

Figure 4. Angular variations of the R1/R1′ ENDOR resonance frequencies in the main crystallographic planes. The EI-EPR spectra along the *a*, *b*, and *c* axes are also shown.

The *g* tensor could only be partially determined from the EI-EPR spectra recorded along the *a*, *b*, and *c* axes ($g = 2.0039$, 2.0034, and 2.0047, respectively).

DFT Hyperfine Coupling Tensor Calculations. Considering the α-L-sorbopyranose structure in Figure 2, as no α-proton hyperfine couplings are observed in the measurements, only radical models that lead to β-couplings need to be considered. In Figure 5, five possible radical models with undisrupted ring structures have been displayed. Radicals formed by hydrogen abstraction at C3, C4, and C5 have been referred to as S−I, S−II, and S−III, respectively. Irradiation products formed by hydroxyl abstraction and by hydroxymethyl group abstraction at C2 have been indicated as models S−IV and S−V, respectively. These models are all proposed under the assumption that no ring openings have taken place, even though this possibility cannot be excluded. Net hydroxyl abstraction from position 2 (S−IV) and net hydrogen abstraction from position 5 (S−III) should in principle yield three β-couplings, and hence, these radicals were not taken to be serious candidates, as was confirmed by DFT calculations. Also the model formed by hydroxymethyl group abstraction from position 2 (S−V), which would yield one β-coupling, was rejected on the basis of the different hyperfine coupling when compared with the experimental data. Summarizing, the radical models S−I and S−II acquired particular attention because both the initial crystallographic C3−H(C4) or C4−H(C3) directions are quite close to the directions associated with the (two) largest β-couplings for R1 and R1′ (see Table 1a): (0.28, 0.75, 0.60) in the crystal as compared to either (0.32, 0.76, 0.57) for R1 and/or (0.33, 0.75, 0.57) for R1′.

The radical at position 4 (S−II) leads to two β-interactions with similar, large isotropic couplings in the range of 70−80 MHz (depending on the approximations made, see below) but with significantly different orientations of the principal axes. This result can be understood by considering Figure 2 where the protons H(C3) and H(C5) are more or less in the same direction with respect to the corresponding carbons, explaining the similarity of the isotropic couplings. The difference in the C4−H(C3) and C4−H(C5) orientations leads to the large difference in the hyperfine coupling tensor principal axes. As these results are not at all compatible with the experimental results, radical model S−II was rejected as a viable candidate structure.

This has, however, considerable importance concerning the similarity between the two β-couplings in Table 1a. Since we found that all candidate models with two nearly identical hyperfine tensors (principal values and axes) in the same radical have to be rejected, and taking into account the apparent doublet nature of the resonance, we can only conclude that the two β-couplings represent the spectral signature of two (very) similar radical structures. A rather obvious opportunity to propose such structures is offered by the A- and B-type sorbose molecules as are shown in Figure 2. Consequently, the radical structure S−I in Figure 5, formed by net H-abstraction at the C3 position, was selected as the starting point for the present DFT investigation. Considering the approach in the "Partial Optimization" scheme, as outlined in the computational details, this means for the current radical model S−I that C3, O3, and H(O3) were

TABLE 1: (a) Experimental Hydrogen Hyperfine Couplings (in MHz) for Radicals R1 and R1′ as Compared with Results from the DFT Calculations (b) Using the Model Structure S−I in Figure 5 for Either A or B Conformations

a.

				eigenvectors			
	A_{iso}	T_{aniso}	A	**a**	**b**	**c**	α[a]
R1 expt		−4.6	62.5	0.77	0.14	−0.62	
	67.1	−2.4	64.7	0.55	−0.64	0.54	
		7.0	74.1	0.32	0.76	0.57	2.9
R1′ expt		−4.6	65.4	0.63	0.28	−0.73	
	70.0	−2.4	67.6	0.70	−0.60	0.38	
		7.0	77.0	0.33	0.75	0.57	3.3
crystallogr. C3−H(C4) direction				0.28	0.75	0.60	

b.

				eigenvectors				
	A_{iso}	T_{aniso}	A	**a**	**b**	**c**	φ_{R1}[b]	φ_{R1}[c]
A No Optim.		−5.1	71.7	0.39	0.48	−0.79	31.2	18.2
	76.8	−1.6	75.2	0.87	−0.48	0.14	31.0	18.3
		6.7	83.5	0.31	0.74	0.60	2.1	2.1
A Part. Optim.		−5.2	83.9	0.52	0.41	−0.75	22.5	9.8
	89.1	−2.4	86.7	0.76	−0.63	0.19	23.5	11.5
		7.6	96.7	0.39	0.66	0.64	8.1	7.4
A Full Optim.		−5.2	49.3	0.50	0.50	−0.71	26.5	14.7
	54.5	−3.5	51.0	0.54	−0.82	−0.20	44.7	37.4
		8.7	63.2	0.68	0.29	0.68	34.5	34.2
B No Optim.		−5.1	72.4	0.40	0.47	−0.79	30.4	17.4
	77.5	−1.7	75.8	0.86	−0.50	0.14	30.3	17.5
		6.8	84.3	0.32	0.73	0.60	2.4	2.1
B Part. Optim.		−4.8	80.8	0.56	0.37	−0.74	19.2	6.5
	85.6	−2.6	83.0	0.73	−0.64	0.23	20.7	9.1
		7.4	93.0	0.39	0.67	0.63	7.4	6.7
B Full Optim.		−4.7	91.6	0.62	0.30	−0.72	13.9	1.3
	96.3	−2.7	93.6	0.64	−0.72	0.26	17.5	10.4
		7.4	103.7	0.44	0.63	0.64	10.9	10.2

[a] This is the angle of deviation (in degrees) between the crystallographic C3−H(C4) direction and the experimentally determined eigenvector for the maximum principal value. [b] This is the angle of deviation (in degrees) between the calculated eigenvector and the corresponding experimental eigenvector from R1. [c] This is the angle of deviation (in degrees) between the calculated eigenvector and the corresponding experimental eigenvector from R1′.

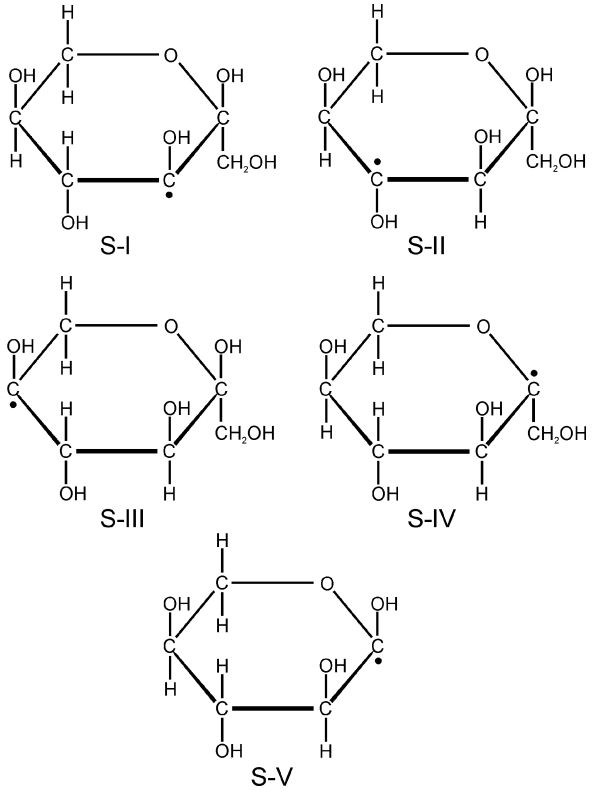

Figure 5. Possible radical models by net hydrogen, hydroxyl and hydroxymethyl group abstraction from the intact sorbose molecule.

allowed to relax, whereas all other atoms of the radical model were maintained at their original positions as in the crystal lattice.

The results of the DFT calculations for the two molecular conformations A and B assuming the radical structure S−I as depicted in Figure 5 are presented in Table 1b. Overall, the experimental R1′ data are in better agreement with the results for both the A and B conformations than are those of R1. However, a slightly better agreement is reached between the "B radical" and R1′, consistently suggesting a hypothetical link between R1 and the "A radical". These assignments are the only ones that seem to make sense, if we attribute the spectral doublet to two separate but similar sorbose radical conformations.

Visual representations of the partially and fully optimized radical conformations A and B are shown in Figure 6. The latter can be compared with the pristine molecular conformations shown in Figure 2. It can be seen in the "Partial Optimization" scheme that only the O3−H(O3) group has moved, whereas in the "Full Optimization" scheme, all atoms in both conformations are rearranged with respect to their positions in the original molecules.

DFT *g* Tensor Calculations. Recently, the option to calculate *g* tensors of free radicals has been implemented in the Gaussian 03 software package.[30] Such calculations were performed on the optimized molecular conformations A and B of radical structure S−I and the results are given in Table 2, together with the *g* values measured along the crystal axes for radical R1 (same as for R1′). These measurements were made using the EI-EPR spectra[37] since the EPR spectra were too complicated due to the multiple radicals present, exhibiting a plethora of overlapping resonance lines. Experimental *g* values were thus only obtained along the crystal axes, and consequently, we have not reported the theoretically predicted principal values but rather the effective *g* values along the crystal axes.

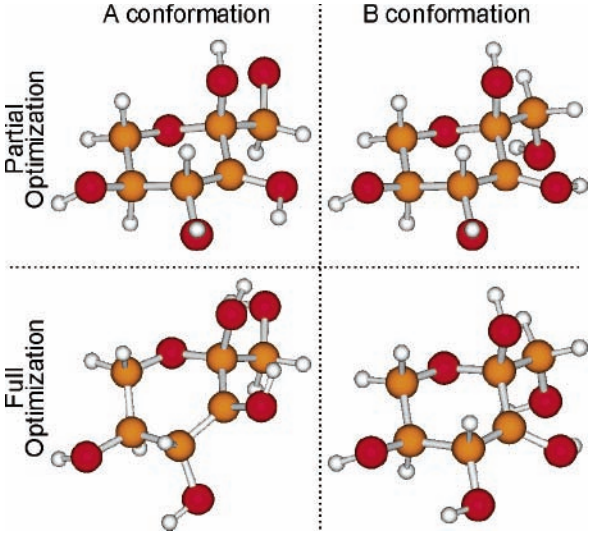

Figure 6. Geometry of the A and B radical conformations after "Partial Optimization" and "Full Optimization".

TABLE 2: DFT Calculated *g* Values for the A- and B-Type Radical Model Structures at Different Levels of Geometry Optimizations, and the Experimental *g* Values for the Radical R1/R1′ Measured along the Crystallographic Axes

		no optimization		partial optimization		full optimization	
	expt[a]	A	B	A	B	A	B
a	2.0039	2.0035	2.0035	2.0031	2.0033	2.0037	2.0030
b	2.0034	2.0026	2.0026	2.0026	2.0025	2.0022	2.0029
c	2.0047	2.0032	2.0033	2.0037	2.0034	2.0035	2.0035

[a] These are experimental *g* values determined from the EI-EPR spectra along the crystallographic axes only. No *g*-tensor analysis has been performed. The estimated uncertainty of the measured values is ±0.0005.

Discussion

Considering first the results from Table 1, it appears that already the pristine crystallographic B conformations of the radical provide excellent agreement between experiment and theory with respect to the direction cosines of the largest coupling ("No Optimization" in Table 1b) for radical R1′. Likewise, both the isotropic and anisotropic hyperfine couplings are reasonably well reproduced. However, the two other principal directions are somewhat less well predicted. A similar comment can be made for the corresponding results for the R1 radical and the A molecular conformation.

It is not unusual that radicals formed by H abstraction from an aliphatic carbon rehybridizes into an sp^2 conformation. Most commonly, this is observed for radical fragments containing an α-hydrogen at the radical center; however, it has recently become clear that even in these cases bending at the radical center occurs more frequently than has previously been assumed.[38] β-type radicals apparently exhibit a less pronounced tendency to rehybridize.[39] Considering the pristine sorbose crystal structure, the dihedral angle θ between the C4−H(C4) bond and the ruptured C3−H(C3) bond direction (the assumed lone electron orbital (LEO) direction) is 4.1° for both the B and A conformations of the sorbose molecules. Dobbs et al. argued that the β-hydrogen hyperfine splitting is rather insensitive to distortions from planarity.[40] This was supported by observations by Madden and Bernhard.[41] As a very rough estimate of the expected β coupling due to unpaired spin density in a LEO that is nearly sp^3 hybrid orbital, one may assume a carbon p orbital (ρ) spin density of about 60%. This is the contribution of the 2p part of the LEO which is the important

part for hyperconjugation, and most of the remaining spin will belong to the 2s component of the orbital and may eventually influence the coupling by spin polarization mechanisms. If the Heller−McConnell relation[42] is approximately valid

$$a_{\mathrm{iso}}^{\beta} = \rho(B_0 + B_2 \cos^2 \theta)$$

an isotropic β coupling of 2.68 mT or 75 MHz for both B and A are obtained, assuming $B_0 = 0$ and $B_2 = 4.5$ mT (that is, 126 MHz;[41,43] Muto[44] derived a value of 120 MHz for the back-lobe hyperconjugation (which is also the case here, see Figure 2) in carboxyl anions). The similarity with the experimental data (67 and 70 MHz for R1 and R1′, respectively), combined with the closeness of the directions of the maximum principal values and the crystallographic C3−H(C4) direction support the supposition that only minor molecular rearrangements have taken place upon radical formation thus clarifying the relative success of the "No Optimization" scheme.

The "Partial Optimization" improves both the anisotropic couplings and the global orientation of the axes set. This is also true for the comparison between the corresponding principal axes of R1′ and B (Table 1), leading to an agreement of the axes within 7°, 9°, and 7°, respectively. However, the isotropic couplings are deviating even further from the experimental values. This is similar to the behavior of the calculated isotropic couplings, using the same method, reported in ref 14. Overall, however, the results of this "Partial Optimization" strategy appear to yield better results than those of the initial structures for both conformations.

The "Full Optimization" leads to even better results in case B where the axes agree within 1°, 10°, and 10°, respectively. The calculated isotropic coupling becomes far worse, however. In case A, on the other side, the fully optimized structure evidently goes out of bounds and is unacceptable. This is already apparent in Figure 6, where the latter conformation is drastically altered with respect to the partially optimized structure.

Comparing the experimental results with the "partially optimized" theoretical results, quantitatively comparable differences are obtained between R1′ and both A and B radical conformations, even though there is a significant discrepancy for the isotropic couplings (see below). Furthermore, the DFT calculations thus give strong support for the radical model of S−I in Figure 5 and the link with the disorder in the sorbose structure. If the difference between the two radicals R1 and R1′ is related to the difference in molecular structure, i.e., the A and B conformations, then the intensity ratio of their spectra should be roughly 0.625/0.375. The latter ratio could unfortunately not reliably be compared with the ENDOR intensity ratios. Furthermore, it could be imagined that there is a further distinction among the A and B related radicals, depending on the neighboring molecules (A or B) at that lattice point. If the disorder is random, then the four (radical-molecule) possibilities, A−A, A−B, B−A, and B−B, have the following probabilities of occurrence: 25/64, 15/64, 15/64, and 9/64, respectively. For the latter calculation, we assumed that only one neighbor molecule influences the radical parameters; this can be rationalized by the fact that only the orientation of the primary alcohol group distinguishes A and B. If the four possibilities lead to distinct hyperfine couplings, then four resonance patterns could be expected. However, regarding the lower probability of the B−B case, we might practically suppose that the latter is not or poorly detectable in the spectra. That leaves the possibility to detect the three other radical-molecule pairs. According to Figure 4, where 3 similar patterns are observed, the principal axes and corresponding dipolar couplings seem rather constant and the differences between the corresponding radicals will be reflected mainly in the isotropic couplings. So, the third (partially detected and nonfitted) angular dependence in Figure 4 is maybe due to, e.g., A−B next to A−A and B−A. A priori we would assume that it is more important if a radical is formed in A or B than the sensitivity of each of these toward whether the neighbor is A or B. As a result with our present knowledge and also considering the incomplete third data set of Figure 4, we prefer the interpretation in terms of only two (A and B) radicals.

The overall agreement between theory and experiment is somewhat less satisfactory than for the radical in glucose[14] where the only significant discrepancy was related to the isotropic couplings. It should be admitted that for the glucose radical the unpaired electron was located in a more rigid molecular environment, far from any rotatable groups. It might be expected that the isotropic couplings can be improved by considering the hydrogen bonds with neighboring sorbose molecules (in particular in the C3, C4 region of the molecule) in more advanced theoretical models as mentioned in refs 27 and 28. Furthermore, such calculations will undoubtedly give further insight in the possible existence of radical−molecule interactions within the crystal.

One should also bear in mind that the present calculations, with their shortcomings, have demonstrated that great care should be taken in how optimizations are performed, as was discussed above. A good illustration of this is the result from the "Full Optimization" scheme for radical A, where the gas-phase optimized structure evidently is far removed from the constrained geometry for the radical in the solid state.

Considering the *g*-tensor calculations, first, it should be noted that for free radicals of this type, aliphatic, nonplanar structures with the major spin density located on carbon atoms and with almost negligible spin densities on heteroatoms having relatively small spin−orbit coupling constants (like oxygen, $\lambda = 151$ cm^{-1}), the *g* shifts are difficult to predict, as they are consisting of a number of small contributions of similar weights. Thus, minor changes in molecular geometry may easily result in large changes in the *g* tensor, particularly with respect to the eigenvectors. This is clearly demonstrated by the results of the calculations presented in Table 2. Second, for determining the experimental *g* values, EI-EPR spectra had to be resorted to, and in these spectra, the two conformations R1 and R1′ are not resolved. Thus, the experimental *g* values reported represent some average of the *g* values for the two radical conformations.

Considering the results in Table 2, it is interesting that all of the *g* values obtained (except maybe for conformation A, full optimization) are in the range of the experimental values and as expected for radicals of this type (see, e.g., the malonic acid radical, $HC^{\cdot}-(COOH)_2$).[37,45] This indicates that DFT-type *g*-tensor calculations may become a useful tool for discussing structures of radicals with more well-defined major contributions to the *g* values. In the present case, the smallest *g* value is consistently obtained along the *b* axis, and for the "Partial Optimization" (which is in the present case better than the "Full Optimization"), the difference between the experimental and calculated values consists only of a systematic shift within the experimental error (Table 2). The difficulty in reproducing the *g* values, probably reflects minor differences between gas-phase (partly) optimized structures and the actual structures in the solid, differences (e.g., −O−H bond conformations mainly determined by hydrogen bonding and other intermolecular contacts in the solid) that are not important for the hyperfine

couplings investigated but which affect the various small contributions to the *g* values.

Conclusions

A new pair of radicals has been identified in X-irradiated sorbose single crystals. The proposed radical model is supported by DFT calculations taking into account the disorder in the sorbose structure. The orientation of the principal axes was attributed a major role in the comparison between experiment and theory.

Acknowledgment. The authors acknowledge the Fund for Scientific Research − Flanders (Belgium) (F.W.O.-Vlaanderen) and the Research Board of the Ghent University.

References and Notes

(1) Stachowicz, W.; Strzelczak-Burlinska, G.; Michalik, J.; Wojtowicz, A.; Dziedzic-Goclawska, A.; Ostrowski, K. *J. Sci. Food Agric.* **1992**, *58* (3), 407.

(2) Ikeya, M. *New applications of electron spin resonance : dating, dosimetry and microscopy*; World Scientific: Singapore, 1993.

(3) Fattibene, P. *Appl. Radiat. Isot.* **1996**, *47* (12), 1375.

(4) Close, D. M. *Radiat. Res.* **1997**, *147* (6), 663.

(5) Debije, M. G.; Bernhard, W. A. *Radiat. Res.* **2001**, *155*, 687.

(6) Becker, D.; Sevilla, M. D. *Adv. Radiat. Biol.* **1993**, *17*, 121.

(7) Ban, F.; Gauld, J. W.; Wetmore, S. D.; Boyd, R. J. In *EPR of Free Radicals in Solids. Trends in Methods and Applications*; Lund, A., Shiotani, M., Eds.; Kluwer Academic Publishers: Dordrecht, The Netherlands, 2003; Chapter 6.

(8) Wetmore, S. D.; Boyd, R. J.; Eriksson, L. A. *J. Phys. Chem. B* **1998**, *102*, 7674.

(9) Vanhaelewyn, G.; Sadlo, J.; Callens, F.; Mondelaers, W.; De Frenne D.; Matthys, P. *Appl. Radiat. Isot.* **2000**, *52*, 1221.

(10) Vanhaelewyn, G.; Lahorte, P.; De Proft, F.; Mondelaers, W.; Geerlings, P.; Callens, F. *Phys. Chem. Chem. Phys.* **2001**, *3*, 1729.

(11) Pauwels, E.; Lahorte, P.; Vanhaelewyn, G.; Callens, F.; De Proft, F.; Geerlings, P.; Waroquier, M. *J. Phys. Chem. A* **2002**, *106* (*51*), 12340.

(12) Madden, K. P.; Bernhard, W. A. *J. Phys. Chem.* **1979**, *83* (20), 2643.

(13) Madden, K. P.; Bernhard, W. A. *J. Phys. Chem.* **1980**, *84* (13), 1712.

(14) Pauwels, E.; Van Speybroeck, V.; Vanhaelewyn, G.; Callens, F.; Waroquier. M. *Int. J. Quantum Chem.* **2004**, Accepted for publication.

(15) Sagstuen, E.; Lund, A.; Awadelkarim, O.; Lindgren, M.; Westerling, J. *J. Phys. Chem.* **1986**, *90* (22), 5584.

(16) Sagstuen, E.; Hole, E. O.; Haugedal, S. R.; Nelson, W. H. *J. Phys. Chem.* A **1997**, *101* (50), 9763.

(17) Heydari, M. Z.; Malinen, E.; Hole, E. O.; Sagstuen, E. *J. Phys. Chem. A* **2002**, *106* (38), 8971.

(18) Malinen, E.; Heydari, M. Z.; Sagstuen, E.; Hole, E. O. *Radiat. Res.* **2003**, *159*, 23.

(19) Kim, S. H.; Rosenstein, R. D. *Acta Crystallogr.* **1967**, *22*, 648.

(20) Nordenson, S.; Takagi, S.; Jeffrey, A. *Acta Crystallogr. B* **1979**, *35*, 1005.

(21) Theisen, H.; Sagstuen, E. *J. Chem. Phys.* **1981**, *74* (4), 2319.

(22) Wetmore, S. D.; Boyd, R. J.; Eriksson, L. A. *J. Phys. Chem. B* **1998**, *102*, 7674.

(23) Ban, F.; Gauld, J. W.; Boyd, R. J. *J. Phys. Chem. A* **2000**, *104*, 5080.

(24) Ban, F.; Gauld J. W.; Boyd R. J. *J. Phys. Chem. A* **2000**, *104*, 8583.

(25) Lahorte, P.; De Proft, F.; Vanhaelewyn, G.; Masschaele, B.; Cauwels, P.; Callens, F.; Geerlings, P.; Mondelaers, W. *J. Phys. Chem. A* **1999**, *103*, 6650.

(26) Lahorte, P.; De Proft, F.; Callens, F.; Geerlings, P.; Mondelaers, W. *J. Phys. Chem. A* **1999**, *103*, 11130.

(27) Pauwels, E.; Van Speybroeck, V.; Lahorte, P.; Waroquier, M. *J. Phys. Chem. A* **2001**, *105*, 8794.

(28) Van Speybroeck, V.; Pauwels, E.; Stevens, F.; Callens, F.; Waroquier, M. *Int. J. Quantum Chem.* **2004**, Accepted for publication.

(29) Frisch, M. J.; Trucks, G. W.; Schlegel, H. B.; Scuseria, G. E.; Robb, M. A.; Cheeseman, J. R.; Zakrzewski, V. G.; Montgomery, J. A., Jr.; Stratmann, R. E.; Burant, J. C.; Dapprich, S.; Millam, J. M.; Daniels, A. D.; Kudin, K. N.; Strain, M. C.; Farkas, O.; Tomasi, J.; Barone, V.; Cossi, M.; Cammi, R.; Mennucci, B.; Pomelli, C.; Adamo, C.; Clifford, S.; Ochterski, J.; Petersson, G. A.; Ayala, P. Y.; Cui, Q.; Morokuma, K.; Malick, D. K.; Rabuck, A. D.; Raghavachari, K.; Foresman, J. B.; Cioslowski, J.; Ortiz, J. V.; Stefanov, B. B.; Liu, G.; Liashenko, A.; Piskorz, P.; Komaromi, I.; Gomperts, R.; Martin, R. L.; Fox, D. J.; Keith, T.; Al-Laham, M. A.; Peng, C. Y.; Nanayakkara, A.; Gonzalez, C.; Challacombe, M.; Gill, P. M. W.; Johnson, B. G.; Chen, W.; Wong, M. W.; Andres, J. L.; Head-Gordon, M.; Replogle, E. S.; Pople, J. A. *Gaussian 98*, revision A.7; Gaussian, Inc.: Pittsburgh, PA, 1998.

(30) Frisch, M. J.; Trucks, G. W.; Schlegel, H. B.; Scuseria, G. E.; Robb, M. A.; Cheeseman, J. R.; Montgomery, J. A., Jr.; Vreven, T.; Kudin, K. N.; Burant, J. C.; Millam, J. M.; Iyengar, S. S.; Tomasi, J.; Barone, V.; Mennucci, B.; Cossi, M.; Scalmani, G.; Rega, N.; Petersson, G. A.; Nakatsuji, H.; Hada, M.; Ehara, M.; Toyota, K.; Fukuda, R.; Hasegawa, J.; Ishida, M.; Nakajima, T.; Honda, Y.; Kitao, O.; Nakai, H.; Klene, M.; Li, X.; Knox, J. E.; Hratchian, H. P.; Cross, J. B.; Adamo, C.; Jaramillo, J.; Gomperts, R.; Stratmann, R. E.; Yazyev, O.; Austin, A. J.; Cammi, R.; Pomelli, C.; Ochterski, J. W.; Ayala, P. Y.; Morokuma, K.; Voth, G. A.; Salvador, P.; Dannenberg, J. J.; Zakrzewski, V. G.; Dapprich, S.; Daniels, A. D.; Strain, M. C.; Farkas, O.; Malick, D. K.; Rabuck, A. D.; Raghavachari, K.; Foresman, J. B.; Ortiz, J. V.; Cui, Q.; Baboul, A. G.; Clifford, S.; Cioslowski, J.; Stefanov, B. B.; Liu, G.; Liashenko, A.; Piskorz, P.; Komaromi, I.; Martin, R. L.; Fox, D. J.; Keith, T.; Al-Laham, M. A.; Peng, C. Y.; Chen, W.; Wong, M. W.; Gonzalez, C.; Pople, J. A. *Gaussian 03*, revision B.03; Gaussian, Inc.: Pittsburgh, PA, 2003.

(31) For an example of a reference work, see: Parr, R. G.; Yang, W. *Density Functional Theory of Atoms and Molecules*; Oxford University Press: New York, 1989.

(32) Krishnan, R.; Binkley, J. S.; Seeger, R.; Pople, J. A. *J. Chem. Phys.* **1980**, *72*, 650.

(33) McLean, A. D.; Chandler, G. S. *J. Chem. Phys.* **1980**, *72*, 5639.

(34) Becke, A. D. *J. Chem. Phys.* **1996**, *104*, 1040.

(35) Close, D. M.; Sagstuen, E.; Hole, E. O.; Nelson, W. H. *J. Phys. Chem. B* **1999**, *103*, 3049.

(36) Vanhaelewyn, G. C. A. M.; Jansen, B.; Callens, F. J.; Sagstuen, E. *Radiat. Res.* **2004**, In press.

(37) Kang, J.; Tokdemir, S.; Shao, J.; Nelson, W. H. *J. Magn. Reson.* **2003**, *165*, 128.

(38) Hosseini, A.; Lund, A.; Sagstuen, E. *Phys. Chem. Chem. Phys.* **2002**, *4*, 6086.

(39) Hole, E. O.; Nelson, W. H.; Sagstuen, E.; Close, D. M. *Radiat. Res.* **1992**, *129*, 119.

(40) Dobbs, A. J.; Gilbert, B. C.; Norman, R. O. C. *J. Chem. Soc. A* **1971**, 124.

(41) Madden, K. P.; Bernhard, W. A. *J. Chem. Phys.* **1979**, *70*, 2431.

(42) Heller, C.; McConnell, H. M. *J. Chem. Phys.* **1960**, *32*, 1535.

(43) Bernhard, W. A. *Adv. Radiat. Biol.* **1981**, *9*, 199.

(44) Muto, H. Trapped anions in organic crystals. In *Radical Ionic Systems*; Lund, A., Shiotani, M., Eds.; Kluwer Academic Publishers: Dordrecht, The Netherlands, 1991.

(45) McConnell, H. M.; Heller, C.; Cole, T.; Fessenden, R. W. *J. Am. Chem. Soc.* **1960**, *82*, 766.